EXPERIMENTAL AND NUMERICAL ANALYSIS OF BUILDING BOUNDARY CONDITIONS

A. Suleiman
University of Tichrin, Faculty of Mechanical and Electrical Engineering, Lattaquié, Syria

A. Trombe
Laboratoire d'Energétique, Université Paul Sabatier, Toulouse, France

Y. Le Maoult and S. Monteix
Centre des Matériaux de l'Ecole des Mines Albi-Carmaux, Albi, France

One of the conditions for the determination of conductive heat transfer through building walls is a knowledge of the heat exchanges at their boundaries and particularly the ra-diative and the convective heat transfer occuring at their surfaces. To study the influence of these two types of heat transfer, the authors have performed a combined experimental and numerical study.

The experimental work consisted of building an experimental setup to satisfy a great variety of boundary conditions that may be encountered on building walls. It was composed mainly of an enclosure, a vertical, heated plate in which natural convection heat flow was generated, and a light source that imposed a known radiative flux condition on the solid surface.

An inverse heat transfer method has also been developed. This numerical method gives the total heat flux leaving the vertical flat plate by conduction, together with surface temperatures. Then it is possible to use a simple thermal balance to determine the radiative and the convective heat flux variations with time. The results of the study are presented together with the corresponding uncertainty calculations. They show that the method could be useful for following heat exchange variations at the solid surfaces of walls.

Several thermal balance models have been developed over recent years, particularly for building applications concerning dwellings equipped with ordinary-sized windows. These thermal balance applications are generally calculated assuming that surface temperatures are uniform. This is not the case if we consider the absorption of the incoming solar direct beam at the solid surface. For this case, boundary conditions can vary with time and intensity if a dynamic process such as a sun patch occurs, even in dwellings filled with obstacles (Figure 1).

Furthermore, this problem is increased in highly glazed enclosures such as verandas or atria, which have become a common feature in building architecture. This type

Address correspondence to Dr. A. Trombe, Director of Thermal and Mechanical Laboratory, Civil Engineering Department, INSA, 135 Avenue de Rangueil, Toulouse Cedex 31077, France. E-mail : trombe@insa-tlse.fr

NOMENCLATURE

a	absorptivity
Bi	Biot number
C_p	heat capacity, J/kg °C
E	density of lighting for calibration, W/m^2
g	gravitational acceleration, m/s^2
Gr	Grashof number
h_{cv}	convective heat transfer coefficient, W/m^2 °C
h_g	global heat transfer coefficient of the copper plate for calibration, W/m^2 °C
m	mass of the copper plate for calibration, kg
q	heat flux density, W/m^2
q_i^{cond}	conductive heat flux density of the ith component, W/m^2
q_i^{cv}	convective heat flux density of the ith component, W/m^2
q_{light}	light flux density, W/m^2
q_i^{rad}	radiative heat flux density of the ith component, W/m^2
S	surface of the copper plate for calibration, m^2
S_i	ith surface area, m^2
t	time, s
T	temperature, °C
Tau	time constant, s
V	volume of the copper plate for calibration, m^3
X_{ij}	sensitivity coefficient
X, Y, Z	Cartesian coordinate system
α	thermal diffusivity, m^2/s
Δ	difference
ε	emissivity
λ	thermal conductivity, W/m °C
ρ	density, kg/m^3
$\overline{\tau}$	normalized representation ratio
Φ_{abs}	radiative flux absorbed by the cooper plate during calibration, W
Φ_{conv}	convective flux emitted by the cooper plate during calibration, W

Superscripts

—	average quantity
$(\ )^T$	transposed quantity

Subscripts

air	ambient condition
surf	surface quantity
abs	absorbed quantity (used only for calibration)

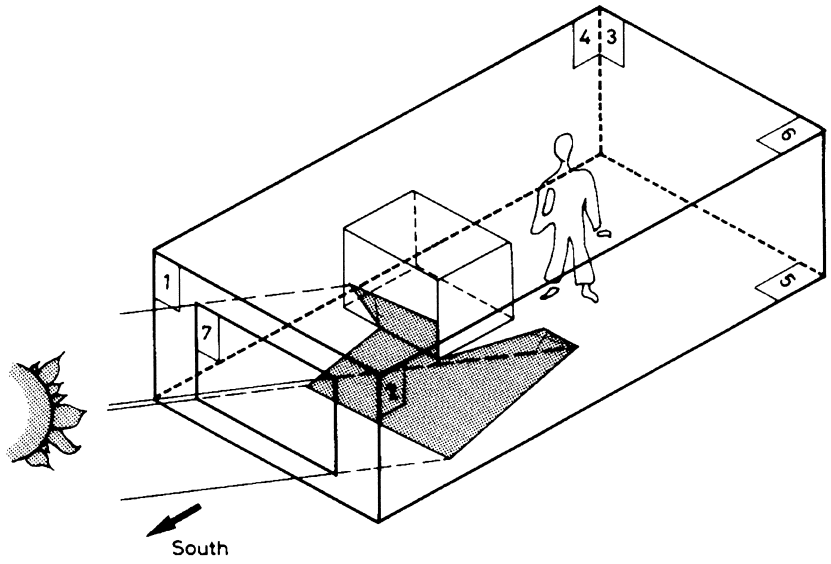

Figure 1. Sun patch problem.

of enclosure, with large volumes that are generally not heated, are subject to large convective and radiative heat exchanges. So these enclosures are difficult to simulate and to design (risks of overheating and comfort problems) if we do not take the incoming solar direct beam into account precisely. That is the reason why our laboratory has developed simulation programs which are now able to give an accurate distribution over time of the different radiative heat fluxes inside these enclosures [1–5]. But we now need to know the impact of the radiative flux on the convective heat exchanges, and this is the main goal of the present research work, based on an original experimental setup.

EXPERIMENTAL SETUP

Description

The experimental setup was composed mainly of an enclosure, a uniformly heated vertical flat plate, and a light source (Figure 2).

The active plate was located inside an enclosure to avoid the influence of external turbulence on the development of the boundary layer. Its dimensions were 1 m height, 0.40 m width, and 0.008 m thickness (resin only). It was composed, from the back face to the front face, of the following components (Figure 3):

An insulating material on all sides except the front face of the plate, to provide adiabatic conditions.
A heat exchanger with hot water circulating at a defined temperature.

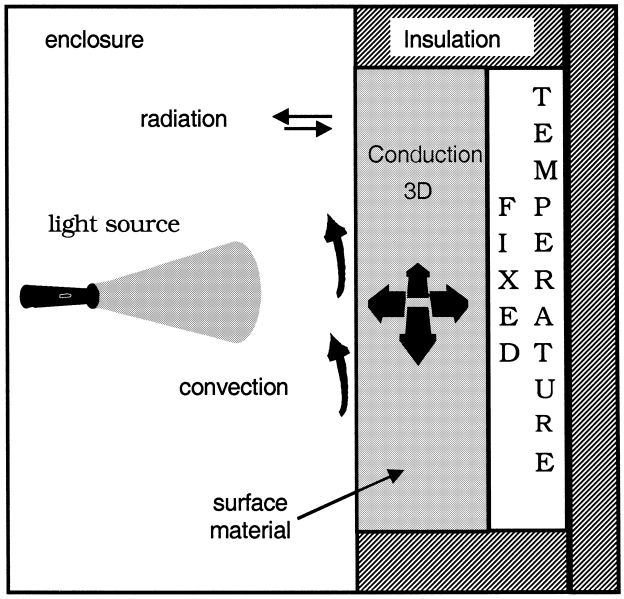

Figure 2. Schematic diagram of the projected study.

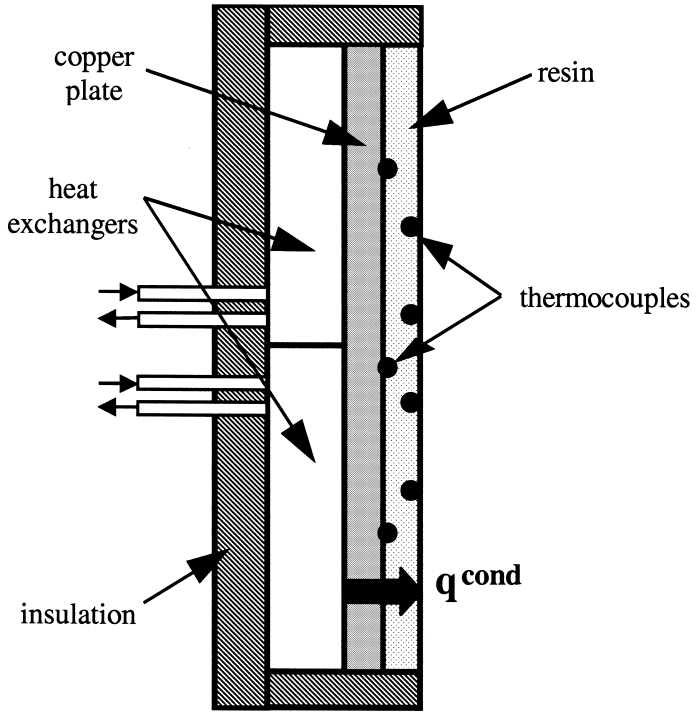

Figure 3. Vertical section of the active plate.

A copper plate to ensure uniform temperatures. On it were fixed several thermocouples so that the temperature imposed at the back face of the resin could be known.

A synthetic material (resin) in which K-type thermocouples with a 0.08-mm mean diameter and a thermal accuracy of $\pm 0.15°C$ were buried.

The back face was in contact with a heat exchanger (in addition to the copper plate), which imposed a fixed boundary temperature at the back of the resin material. Radiative and convective heat transfer occurred at the front face.

The light source was also built for this experiment. It was composed of an insulated box made of aluminum, in which several short infrared lamps were located (Figure 4).

The surface temperature of the protection enclosure was also measured so that radiative exchanges could be calculated. It should be noted that surfaces having high emissivity coefficients ($\varepsilon > 0.9$) were chosen in order to correspond to those classically encountered in building enclosures.

Optimization

Front face material of the plate. Preliminary numerical studies were necessary to optimize both the choice of the front face material and the location of the thermocouples

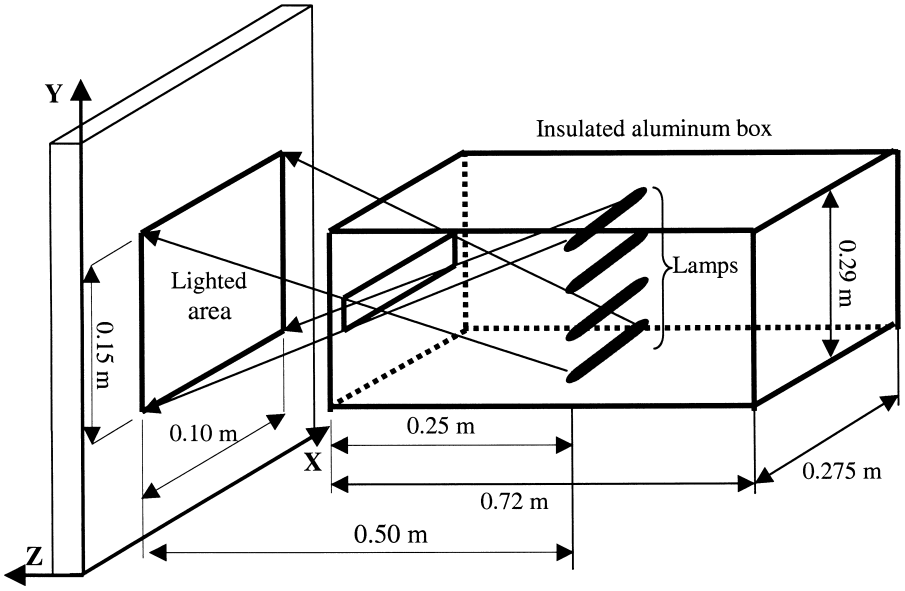

Figure 4. Diagram of the radiative heat source.

inside it. To do this, we used a method developed by Blanc [6]. It is based on a quantity called the normalized ratio of representation, which is defined as

$$\overline{\tau} = \frac{\tau_j}{\tau_{\max}} \tag{1}$$

where

$$\tau_j = \sum_{i=1}^{m} X_{i,j} \qquad \text{for } j = 1 - n$$

$$\tau_{\max} = \operatorname{Max}(\tau_j) \qquad \text{for } 1 \leq j \leq n$$

This ratio allows the sensitivity of the sensor to a flux density to be determined according to the location where it is used. The sensor location method consists of successive trials to find the locations that satisfy relationship (2):

$$\forall j \qquad 0.75 \leq \overline{\tau} \leq 1 \tag{2}$$

It is important to obtain a uniform value of the normalized representation ratio. We studied several types of building materials for the surfaces, namely, plaster, wood, and insulation materials. We finally chose a synthetic resin having thermophysical properties suitable for the planned studies (Table 1). This material presents two advantages. First, it has a good insulation coefficient that keeps its sensitivity coefficient values high. Second,

Table 1. Thermophysical properties of the resin

Material	Coefficient of conductivity (W/m °C)	Heat capacity (J/kg °C)	Density (Kg/m^3)	Emissivity
Resin	0.06	1,454	480	0. 95

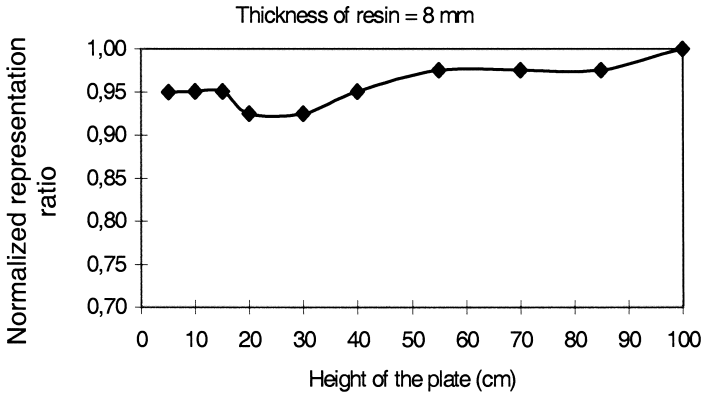

Figure 5. Normalized representation ratio of thermocouples buried in the resin.

its heat capacity is sufficient and very similar to the heat capacity of plaster. Therefore, the thermocouples were located inside that material in order to reach high values of the normalized representation ratio (Figure 5).

Radiative source. The location of the lamps inside the box was optimized in order to obtain a uniformly lighted area. This work, which is not presented here, was done in collaboration with the Ecole des Mines of Albi [7]. Here we present only the process of calibration and its final result.

A very thin copper plate, covered by a defined black paint, was used to calibrate the power of the infrared lamp system (Table 2). This copper plate was placed between the lamp system and an infrared camera. We considered that the plate temperature variation was uniform as the copper plate satisfied a Biot number condition (Bi $<$ 0.1). To determine the radiation power of this system, we recorded with the infrared camera, the

Table 2. Thermophysical properties of the copper plate used for calibration

Material	Thickness (m)	Surface area (m^2)	Coefficient of conductivity (W/m °C)	Heat capacity (J/kg °C)	Density (kg/m^3)	Absorptivity
Copper	0.0003	0.001583	380	383	8,900	0.92

time variation $T(t)$ of the copper plate temperature field. We did this for several supply voltages of the lamps (Figure 6).

The plate temperature variation (internal energy) may be represented by the following thermal balance:

$$\rho V C_p \frac{dT}{dt} = \Phi_{\text{conv}}(t) + \Phi_{\text{abs}}(t) \tag{3}$$

Replacing the convective and the radiative terms by their values, we obtain

$$\rho V C_p \frac{dT}{dt} = -2h_g S(T - T_{\text{air}}) + aES \tag{4}$$

This first-order differential equation admits a solution of the type

$$T = T_{\text{air}} + \frac{\Phi_{\text{abs}}}{2h_g S}(1 - e^{t/\text{Tau}}) \tag{5}$$

where $\text{Tau} = mC_p/(2h_g S)$ is the time constant.

By derivation of Eq. (5) with the respect to time, we can reach the value of the flux absorbed by the copper plate:

$$\Phi_{\text{abs}} = mC_p \left(\frac{dT}{dt}\right)_0 \tag{6}$$

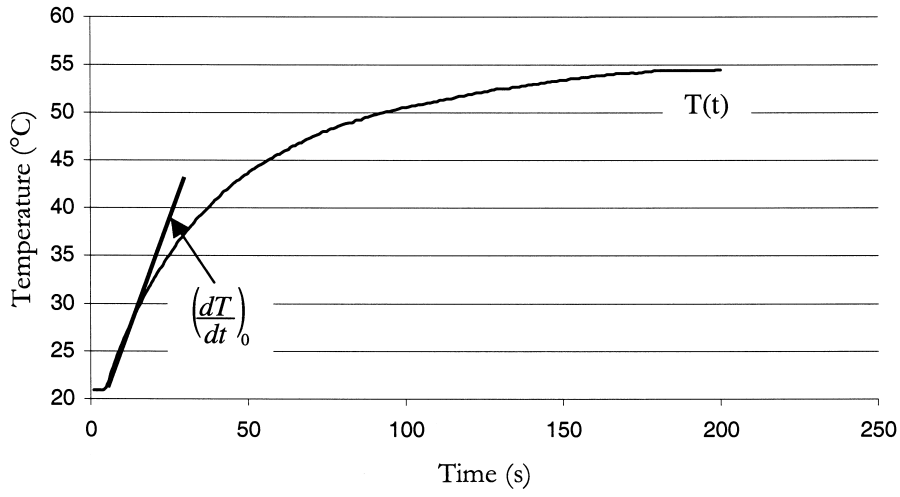

Figure 6. Experimental temperature variation of the copper plate used for calibration.

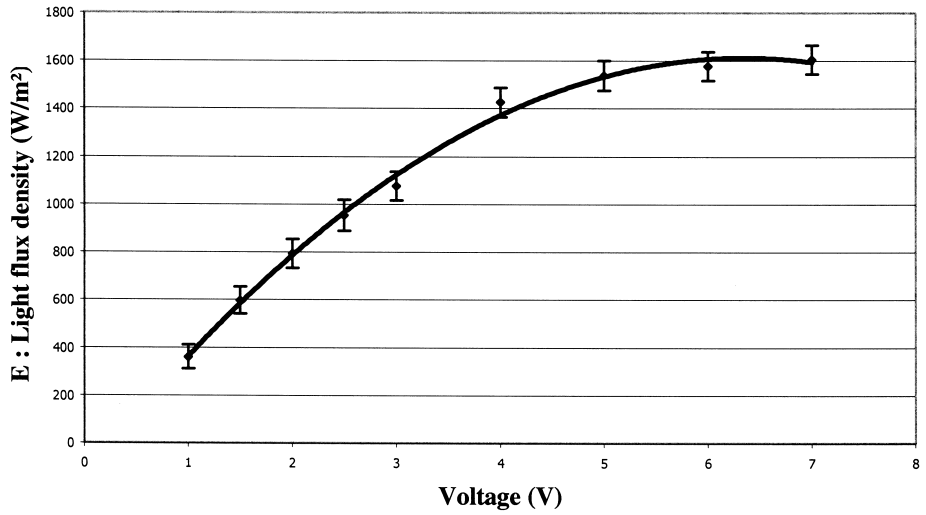

Figure 7. Power of the radiative system.

The factor $(dT/dt)_0$ in Eq. (6) represents the slope of the copper plate temperature with variation time when the lamp system is lighted. It corresponds to the linear part of the $T(t)$ curve at the first moments of lighting; see Figure 6. The knowledge of that slope finally led to the value of the light flux density of the radiative source, Eq. (7):

$$E = \frac{mC_p(dT/dt)_0}{aS} \tag{7}$$

The results of calibration are given in Figure 7 for each supply voltage of the lamps. The uncertainty bars are calculated as described in Appendix A.

The light flux density was limited by one factor, which corresponded to the distance between the front side of the aluminum box and the lighted area represented by the resin. In fact, it was necessary to keep a sufficient distance between these two elements to avoid perturbations of the convective heat flow generated by the uniformly heated vertical flat plate. Consequently, the possibilities of the radiative system were reduced to a variable power within the range 0–170 W/m^2.

NUMERICAL METHOD

The numerical method developed for this work was based on the inverse identification method presented in [8, 9]. We give a brief review of the main steps of this method below.

1. The numerical solution of the direct problem was based on a finite-difference technique [10]. This was a three-dimensional model because, for the sun patch study, we needed to know the temperature distribution inside the plate in all directions. Therefore, we stated the boundary conditions of our plate in a three-dimensional Cartesian system

of coordinates. The mathematical representation is

$$\begin{cases} \alpha\left(\dfrac{\partial^2 T}{\partial x^2}+\dfrac{\partial^2 T}{\partial y^2}+\dfrac{\partial^2 T}{\partial z^2}\right)=\dfrac{\partial T}{\partial t} \\ \text{for } z=0, -\lambda\left.\dfrac{\partial T}{\partial z}\right|_{z=0}=q_i^{\text{cond}} \\ \text{for } z=(\text{Thickness})\ T=T_1, \forall x, y=\text{known} \\ \text{at } x=0 \text{ and } x=\text{Width}, \dfrac{\partial T}{\partial x}=0, \forall y, z \\ \text{at } y=0 \text{ and } y=\text{Height}, \dfrac{\partial T}{\partial y}=0, \forall x, z \end{cases} \tag{8}$$

2. The heat transfer flux at the solid surface was the sum of the radiative and the convective effects, so the inverse problem was nonlinear. Furthermore, the heat transfer was also a function of the local surface temperature distribution. To take these phenomena into account, a linear inverse method elaborated by Taler [11] was chosen, and we used the following hypotheses.

The global heat flux q_i^{cond} leaving the front face was divided into n components $q_1, q_2, \ldots, q_n$ along the Y coordinate (Figure 8).

Consequently the radiative q_i^{rad} and the convective q_i^{cv} heat fluxes were also divided into n components.

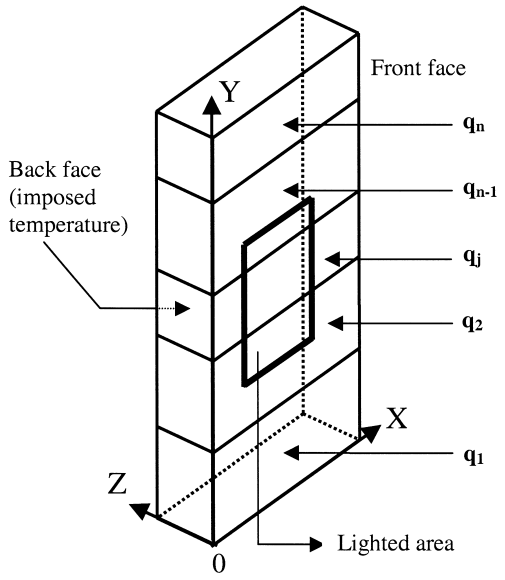

Figure 8. Theoretical division of the active plate.

3. The numerical solution of this problem was found by a minimization process between the experimental temperatures given by the thermocouples buried inside the resin and the numerical temperatures calculated by the model. As it was an iterative process, it was solved again for new flux values until the variation between two calculation steps reached a low value, i.e., Eq. (9):

$$\left| \frac{q_j^{k+1} - q_j^k}{q_j^k} \right| < \varepsilon \qquad \text{for } j = 1, \ldots, n \tag{9}$$

4. The use of the inverse method also led to the knowledge of the average surface temperature of each component of the active plate. Therefore, before determining the convective heat flux, it was first necessary to calculate the radiative heat flux for each component of the plate. This was done using the classical radiosity method [12, 13].

5. Finally, to determine the radiative and the convective fluxes of each component, on the front face of the plate, we applied the following two thermal balances.

The first corresponds to locations outside the lighted area,

$$q_i^{\text{cond}} = q_i^{\text{cv}} + q_i^{\text{rad}} \tag{10}$$

The second corresponds to locations inside the lighted area,

$$q_i^{\text{cond}} + a \times q_{\text{light}} = q_i^{\text{cv}} + q_i^{\text{rad}} \tag{11}$$

RESULTS

Presentation of the Results

The results presented here concern unsteady-state variations of experimental parameters (buried thermocouples) or values calculated by the model. For this study the active plate was divided into 12 components, of which four were located inside the lighted area (Figure 9).

Various boundary conditions were tested. They corresponded to:

A light flux density of 166 W/m^2 applied to the front face of the resin for 220 s
Different temperatures imposed at the back face of the resin, allowing temperature differences $\Delta T = \overline{T}_{\text{surf}} - \overline{T}_{\text{air}}$ within the range 2.7–14.7°C.

Experimental Analysis of Thermocouple Behavior

We first present an experimental analysis corresponding to the temperature variations of the thermocouples numbered 29, 32, 34, and 49, located inside the lighted area (Figure 10).

Figure 10 shows the temperature variations of the thermocouples with the duration of illumination. During the illumination, the temperature varied in the range 28.5–32.5°C for all the sensors. However, two types of thermocouple thermal behavior may be distinguished. The first corresponds to thermocouples 49 and 32, located in the central part of the lighted area. These thermocouples presented the greatest amplitude of variation.

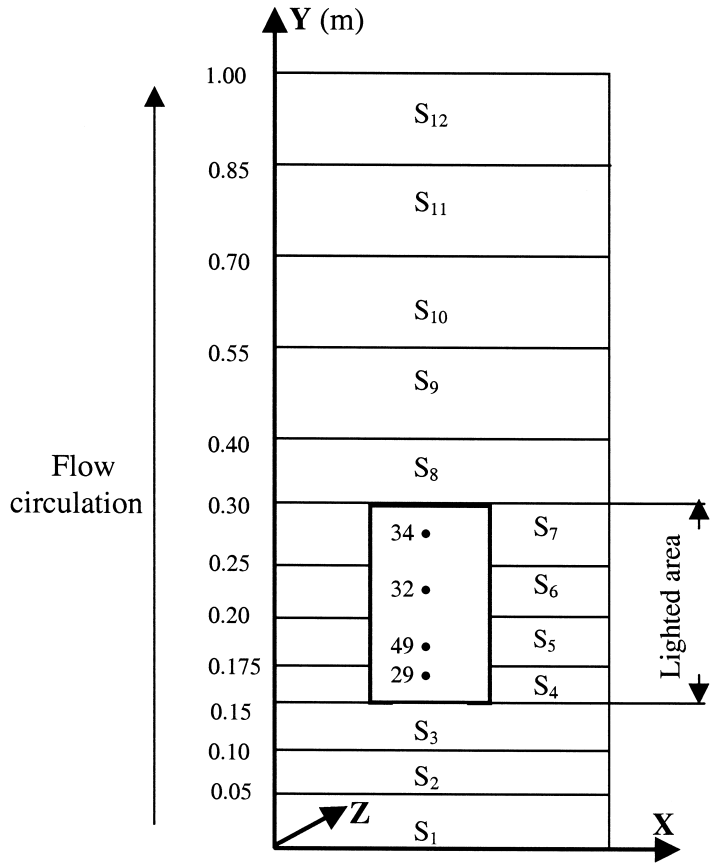

Figure 9. Division of the active plate into components, and location of the thermocouple sensors (•) inside the lighted area.

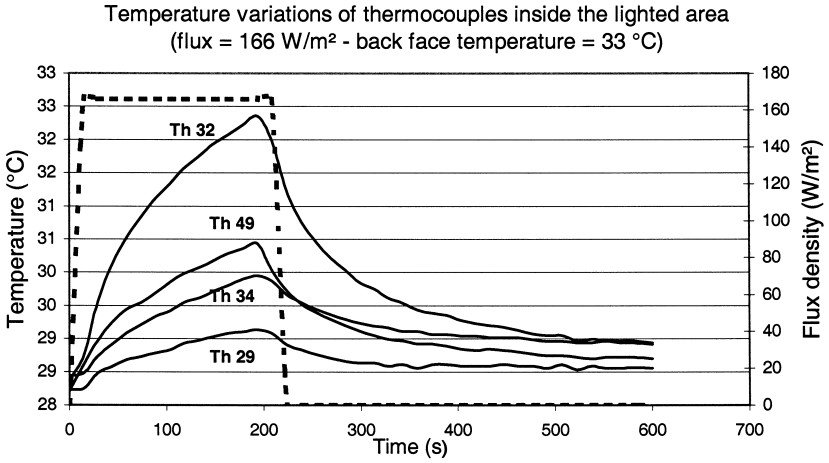

Figure 10. Experimental temperature variations of thermocouples located inside the lighted area.

Table 3. Characteristics of the configuration studied

$\overline{T}_{air}$ (°C)	$\overline{T}_{surf}$ (°C)	$\Delta T = \overline{T}_{surf} - \overline{T}_{\infty}$ (°C)	$\overline{Gr} = \beta g \Delta T \frac{H^3}{v^2}$
23.7	(31.1–32.0)	(7.4–8.3)	(8.99–10.05) $\times$ 10^8

The second is relative to the two thermocouples located at the limits of the lighted area (bottom or top). In this case the variation amplitudes of the two thermocouples (29 and 34) were lower. The reason is that the energy emitted by the radiative source and absorbed by the resin is diffused toward the nonlighted area. Note that this thermal behavior was confirmed for all other experimental conditions used during this experimental work.

Conductive, Convective, and Radiative Variations

We chose experimental conditions that were representative of the general thermal behavior of the conductive, radiative, and convective fluxes. They were a light flux density of 166 W/m^2 and other conditions as indicated in Table 3.

The variations with time of six components are drawn in Figures 11, 12, and 13. Four were located inside the lighted area (components 4, 5, 6, and 7), the two others (components 1 and 12) being outside that area at the bottom and at the top of the active plate, respectively.

Concerning the variation of conductive heat fluxes of the lighted components (4–7) we see (Figure 11) that they decrease from the first moments of lighting. This phenomenon corresponds to flux inversions which depend on the component locations. Then, just after the extinction of the radiative source, the conductive flux increases rapidly and reaches higher values during the heat restitution because the material had stored heat in the previous periods.

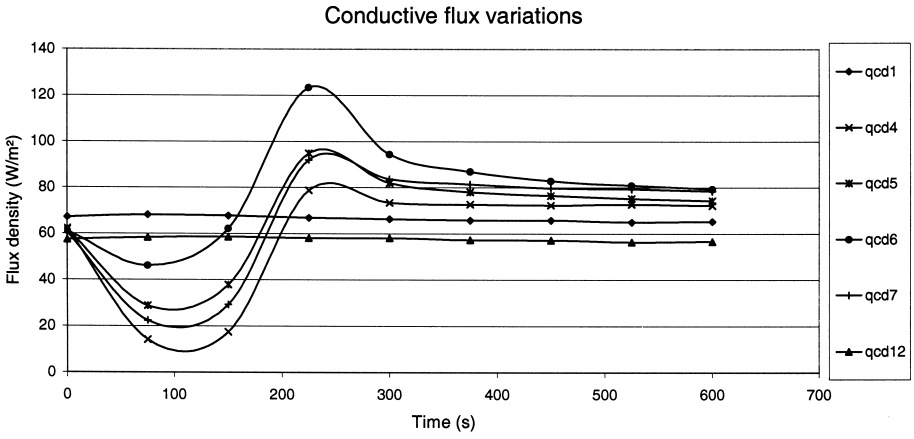

Figure 11. Conductive heat flux variations with time for $7.4 < \Delta T < 8.3$°C.

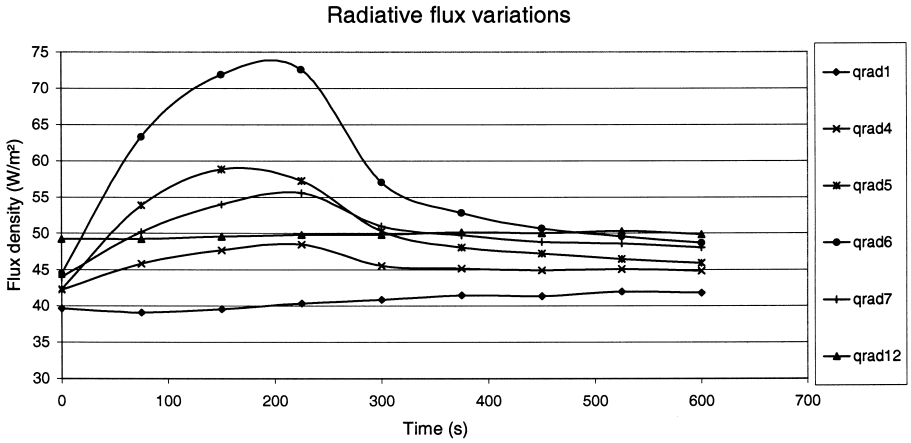

Figure 12. Radiative heat flux variations with time for $7.4 < \Delta T < 8.3°C$.

Note that components 1 and 12, not located in the lighted area, do not exibit significant variation during the lighting period.

Figures 12 and 13, for the radiative and convective heat exchanges, show that the variations of components 4, 5, 6, and 7, located inside the lighted area, are significant. Nevertheless, if we compare these two heat exchanges occurring at the solid surface, the followings observations can be made.

1. The order of variations between the different components of the lighted area is respected. The central components (5 and 6) of the lighted area present the greatest temperature variations. For the other two, located at extreme positions (components 4 and 7), the variations are lower. We note again here, as mentioned

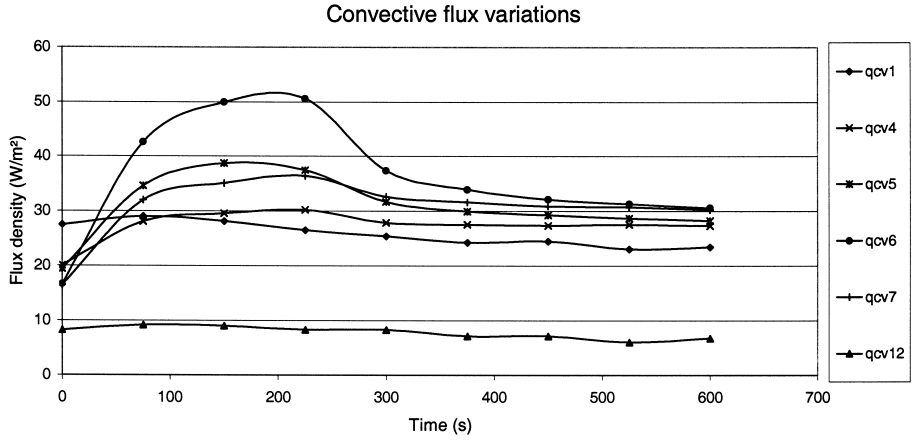

Figure 13. Convective heat flux variations with time for $7.4 < \Delta T < 8.3°C$.

earlier, that the energy emitted by the radiative source and absorbed by the resin is diffused toward the nonlighted area.

2. The amplitudes of variations are different between the two types of exchanges. Due to the illumination, the convective heat exchange varies by more than twice its initial value before lighting. This is the case for the three upper components located in the lighted area, except for component q_{cv4}. This may be explained, on the one hand, by the heat restitution of the energy stored in the resin during lighting, and, on the other hand, by the increase in air temperature due to convection effects from the bottom to the top of the plate.

Finally, if we consider now the two components (1 and 12) not located in the lighted area, we see that the illumination does not affect their variation in a significant manner. Nevertheless, a very slight variation may be observed, certainly due to the reflections of beam from the radiative source inside the enclosure.

Convective Heat Exchange Variations

Figure 14 shows the variations of convective heat exchange coefficients with time. These coefficients were calculated using the convective fluxes given by the inverse method and in terms of the average temperature difference $\Delta T = \overline{T}_{surf} - \overline{T}_{air}$ for each component of the lighted area. Of course, we see again the flux variations corresponding to the variations of thermocouples already recorded in Figure 10.

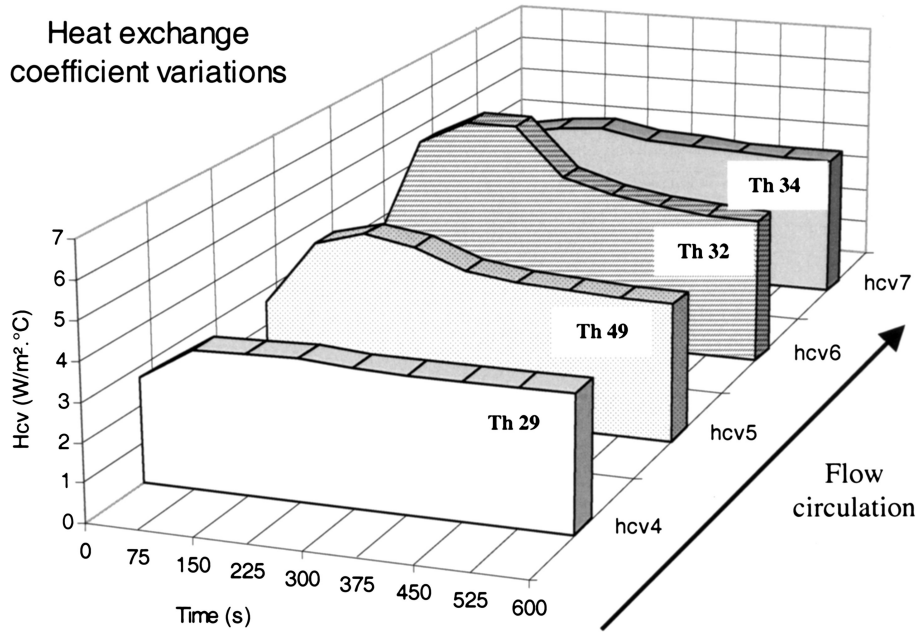

Figure 14. Convective heat exchange variations of the lighted components for an average temperature difference $7.4 < \Delta T < 8.3°C$.

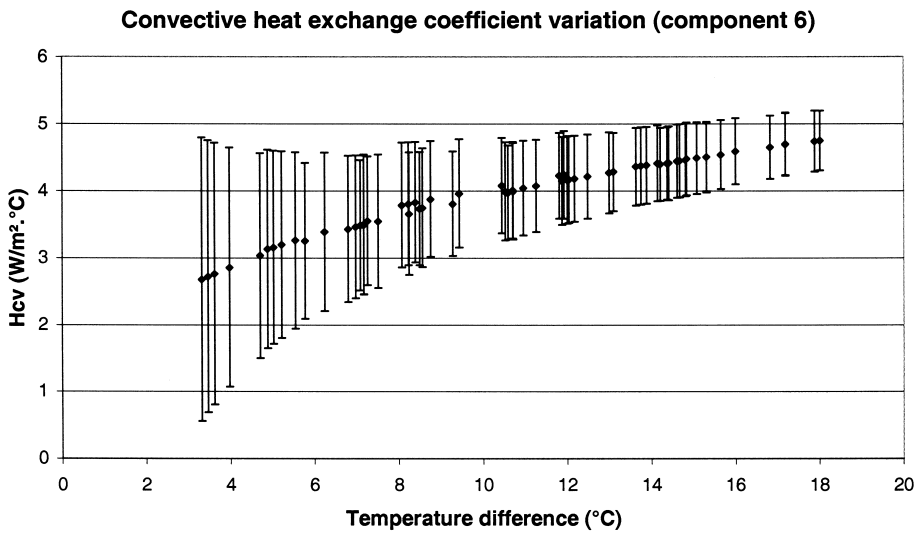

Figure 15. Values of the convective heat exchange coefficient of component 6.

If we consider now the highest variation, represented by the component H_{cv6} (component 6, Th 32), we see that this variation can reach more than 50% of its initial value before illumination (Figure 15). Figure 15 indicates, as was foreseeable, that uncertainties (calculated in Appendix B) are high for weak values of convective heat exchanges. This fact points out the weakness of the thermal balance method for such values.

Heat Exchange Convective Law

The observation of two facts allowed us to propose a global convective heat exchange law for the lighted area.

1. The temperature variations observed, Figure 10, for all the components are very similar.
2. The convective heat exchange variation is also similar to that observed (Figure 15) for all the other components located in the lighted area.

Consequently, this law was determined in terms of the average temperature difference $\Delta T = \overline{T}_{surf} - \overline{T}_{air}$ for all the components of the lighted area, Eq. (12):

$$h_{cv} = 1.83 \times (\overline{T}_{surf} - \overline{T}_{air})^{0.33} \tag{12}$$

Note that this law has a power coefficient of 0.33. According to the literature, e.g., [14, 15], this indicates a situation of turbulent flow. However, we cannot conclude this with certainty because, during the lighting period, the Grashof number varies with the increase of surface temperature and we may encounter several flow regimes.

CONCLUSION

In this study, experimental variations and results obtained by numerical works have been presented. They show the interest in developing (optimizing) and conducting these two types of works simultaneously.

The results demonstrate that the inverse method is pertinent, even if it is subject to considerable uncertainties, particularly when the convective heat exchanges take weak values. Nevertheless, this method based on a simple thermal balance is easy to develop and may be used to obtain approximate evaluations of heat exchange coefficients. It may be interesting particularly to follow unsteady-state variations of convective heat exchange coefficients in real buildings on site.

The different algorithms and models developed for the study are robust. They may be used for other types of applications. We have particularly in mind industrial processes such as the thermoforming of plastic bottles, which needs higher levels of temperature.

REFERENCES

1. A. Mavroulakis, J. M. Baleynaud, R. Javelas, and A. Trombe, Dynamic Processing of Direct Solar Gains in T.R.N.S.Y.S Building Simulation Environment, ISES Solar Congress, Denver, CO, 17–24 August, 1991.
2. R. Kraus, E. R. F. Winter, and W. Ebele, Investigation of the Energy Flows for Transparent Building Façade, *Solar Energy*, vol. 51, no. 6, pp. 481–493, 1993.
3. P. Pfrommer, Thermal Modelling of Highly Glazed Spaces. Ph.D. thesis, Monfort University, Leicester, U.K., 1995.
4. A. Mavroulakis, Développements d'outils destinés à la modélisation des échanges radiatifs dans des enceintes de géométrie complexe. Calcul de facteurs de forme en présence d'obstacles, Ph.D. thesis, University P. Sabatier, Toulouse, France, 1995.
5. L. Serres, Etude de l'impact d'une perturbation thermique locale de type tache solaire, Influence sur le confort thermique, Ph.D. thesis, INSA, Toulouse, France, 1997.
6. G. Blanc, Problèmes inverses multidimensionnels de conduction de la chaleur. Optimisation du positionnement des capteurs et utilisation des mesures de thermo-déformations, Ph.D. thesis, INSA, Lyon, France, 1996.
7. S. Monteix, Modélisation du chauffage convecto-radiatif de préformes en P.E.E.T. pour la réalisation de corps creux, Ph.D. thesis, ENSTIMAC, Paris, Albi, France, 2001.
8. I. Cuniasse-Langhans, Evaluation par méthode inverse de la distribution de flux de chaleur pariétaux le long d'une plaque plane verticale en convection naturelle, Ph.D. thesis, INSA, Toulouse, France, 1998.
9. I. Cuniasse-Langhans, A. Trombe, J. Dumoulin, and M. Begue, Efficiency of an Inverse Method to Determine Natural Convection Heat Transfer, *Numer. Heat Transfer B*, vol. 39, no. 6, pp. 603–615, 2001.
10. Y. Jaluria and K. E. Torrance, *Computational Heat Transfer*, Hemisphere, Washington, DC, 1986.
11. J. Taler, Nonlinear Steady-State Inverse Heat Conduction Problem with Space-Variable Boundary Conditions, *J. Heat Transfer*, vol. 114, pp. 1048–1051, 1992.
12. R. Siegel and J. R. Howell, *Thermal Radiation Heat Transfer*, 3d ed., Hemisphere, Washington, DC, 1992.
13. E. M. Sparrow, On the Calculation of Radiant Interchange between Surfaces, in *Modern Developments in Heat Transfer*, pp. 181–211, Academic Press, New York, 1963.
14. A. Bejan, *Convective Heat Transfer*, Wiley, New York, 1995.
15. A. Bejan, *Heat Transfer*, Wiley, New York, 1993.
16. J. V. Beck and K. J Arnold, *Parameter Estimation in Engineering and Science*, Wiley, New York, 1977.

APPENDIX A

The power of the radiative source was determined experimentally. Consequently, it was subject to the following uncertainties.

Uncertainty in the measurement by voltmeter of the supply voltage of the lamps. The accuracy of this apparatus, at a temperature of $23 \pm 5°C$ and for a voltage of 7 V (the case of our experimentation), is $\Delta V = \pm 1.6325 \times 10^{-4}$ V. As that uncertainty is very small, we neglected it.

Uncertainty in the surface temperature measurement of the copper plate for calibration. If we assume that the lighting is given by Eq. (7), the relative uncertainty on that value is given by

$$\frac{\Delta E}{E} = \frac{\Delta(\Delta T)}{T} + \frac{\Delta(\Delta t)}{t}$$

The second term can be neglected, given the high acquisition frequency of the infrared camera. Therefore, the uncertainty on the lighting is reduced to an uncertainty depending only on the measured temperature:

$$\frac{\Delta E}{E} = \frac{\Delta(\Delta T)}{T}$$

If we accept that T_{measured} is given by the expression below, the uncertainty on the surface temperature measurement is reduced to the dynamic and calibration uncertainties.

$$T_{\text{measured}} = T_{\text{black body}} \pm |\Delta T_{\text{dynamic}}| \pm |\Delta T_{\text{calibration}}| \pm |\Delta T_{\text{black body}}|$$

Then

$\Delta T_{\text{dynamic}} = 3 * \text{DTEB}$ (equivalent noise temperature discrepancy)
$\Delta T_{\text{calibration}} = 0.25°C$ (measured on the calibration total characteristic of black body)
$\Delta T_{\text{black body}} = 0$ because neglected

APPENDIX B

The uncertainty calculations of the convective heat exchange coefficients, in unsteady state, were determined from Eq. (11):

$$q_i^{\text{cond}} + a \times q_{\text{light}} = q_i^{\text{cv}} + q_i^{\text{rad}} \tag{11}$$

Note that this expression depends on different parameters that enter into the thermal balance of the lighted area. Two literal expressions are necessary to reach this type of result.

The first gives the relative uncertainty on the convective heat flux:

$$\left(\frac{\Delta\varphi_{\text{cv}}}{\varphi_{\text{cv}}}\right)_{\text{max}} \leq \left|\frac{\Delta\varphi_{\text{total}} + \Delta\varphi_{\text{rad}} + \Delta\varphi_{\text{abs}}}{\varphi_{\text{total}} + \varphi_{\text{abs}} - \varphi_{\text{rad}}}\right|$$

The second gives the relative uncertainty on the heat exchange coefficient from the classical law heat transfer by convection:

$$\left(\frac{\Delta h_{cv}}{h_{cv}}\right)_{max} = \sqrt{\left(\frac{\Delta \varphi_{cv}}{\varphi_{cv}}\right)^2_{max} - 2\left(\frac{\delta T}{\Delta T}\right)^2}$$

For these calculations, we took the following parameter uncertainties into account.

- The absolute uncertainty on thermocouple accuracy is $\pm$ 0.15°C. Note that this type of error occurs in the calculation of the different flux components and we took this fact into account.
- Concerning conductive exchanges, the location uncertainty of thermocouples inside the resin was taken as 0.1 mm. We assumed that it was equivalent to a temperature uncertainty.
- Concerning radiative exchanges, the relative uncertainty on view factors = 1% (from numerical data); and the relative uncertainty on emissivity coefficient = 2% (from experimental data).

Generally speaking, these calculations were done using a Monte Carlo method [16]. We followed the different stages.

1. With the help of a random noise generator and assuming a Gauss law probability distribution, we can draw m values of the random variable $\delta(T)$ of temperature error.
2. These values are added to numerical temperatures given by the model to obtain noised temperatures.
3. Finally they are injected into the numerical model to obtain a first evaluation of the total flux component q_i^{cond}, for example.

Stages 2 and 3 were repeated N times ($N \geq 50$) to reach a statistical evaluation of the uncertainty.